HYDROLOGICAL PROCESSES
Hydrol. Process. **29**, 965–978 (2015)
Published online 7 May 2014 in Wiley Online Library
(wileyonlinelibrary.com) DOI: 10.1002/hyp.10209

Groundwater temperature evolution in the subsurface urban heat island of Cologne, Germany

Ke Zhu,[1,3] Peter Bayer,[2]* Peter Grathwohl[1] and Philipp Blum[3]

[1] *Center for Applied Geosciences (ZAG), University of Tübingen, Hölderlinstr. 12, 72074, Tübingen, Germany*
[2] *Department of Earth Sciences, ETH Zurich, Sonneggstrasse 5, 8092, Zurich, Switzerland*
[3] *Institute for Applied Geosciences (AGW), Karlsruhe Institute of Technology (KIT), Kaiserstraße 12, 76131, Karlsruhe, Germany*

Abstract:

Long-term heating of shallow urban aquifers is observed worldwide. Our measurements in the city of Cologne, Germany revealed that the groundwater temperatures found in the city centre are more than 5 K higher than the undisturbed background. To explore the role of groundwater flow for the development of subsurface urban heat islands, a numerical flow and heat transport model is set up, which describes the hydraulic conditions of Cologne and simulates the transient evolution of thermal anomalies in the urban ground. A main focus is on the influence of horizontal groundwater flow, groundwater recharge and trends in local ground warming. To examine heat transport in groundwater, a scenario consisting of a local hot spot with a length of 1 km of long-term ground heating was set up in the centre of the city. Groundwater temperature-depth profiles at upstream, central and downstream locations of this hot spot are inspected. The simulation results indicate that the main thermal transport mechanisms are long-term vertical conductive heat input, horizontal advection and transverse dispersion. Groundwater recharge rates in the city are low ($<100\,\mathrm{mm\,a^{-1}}$) and thus do not significantly contribute to heat transport into the urban aquifer. With groundwater flow, local vertical temperature profiles become very complex and are hard to interpret, if local flow conditions and heat sources are not thoroughly known. Copyright © 2014 John Wiley & Sons, Ltd.

KEY WORDS subsurface urban heat island (UHI); simulation; groundwater temperature-depth (GWTD) profile; dispersion; Cologne

Received 1 October 2013; Accepted 26 March 2014

INTRODUCTION

In the last century, a strong warming trend in urban subsurface has been revealed in many large cities such as Tokyo, Bangkok and Berlin (Taniguchi *et al.*, 2007; Menberg *et al.*, 2013a). Field studies in North America (Wang *et al.*, 1994; Ferguson and Woodbury, 2007), Europe (Balke, 1977; Bodri and Cermak, 1997; Perrier *et al.*, 2005; Menberg *et al.* 2013a) and Asia (Taniguchi *et al.*, 2007; Huang *et al.*, 2009; Yamano *et al.*, 2009) have indicated a rise of the regional urban underground temperature by 2–5 K. The factors that raise the atmospheric temperature in cities and lead to the evolution of atmospheric urban heat islands (UHIs) are also responsible for ground warming. These factors are, for example, solar heating of massive urban structures, such as buildings, and sealed surfaces, such as roads. UHIs in the subsurface are augmented by further non-climatic perturbations, such as in-ground heat losses from buildings, landfills, underground parking lots and subway tunnels, as well as from buried electrical power lines, district heating networks, sewage water canals and leakages (Balke, 1977; Pollack *et al.*, 1998; Menberg *et al.*, 2013b).

Temperature fluctuations at the surface or in shallow depth penetrate further into the ground. They can be seen in deeper borehole temperature logs as deviation from the unperturbed, natural temperature profiles (Huang *et al.*, 2000; Taniguchi *et al.*, 2007). Numerous studies in borehole climatology examined vertical temperature logs that are not suspected of being affected by non-climatic factors. Most of them identified a warming trend and increasing downward heat flux during the last century (e.g. Pollack *et al.*, 1998; Huang *et al.*, 2000; Perrier *et al.*, 2005). Only a few focused on perturbed profiles (e.g. Taniguchi *et al.*, 1999; Gunawardhana and Kazama, 2011). Urban ground surface temperature history was interpreted, for example, by Yamano *et al.* (2009), who logged more than 100 boreholes of generally 100–250 m depth in the Asian megacities Bangkok, Jakarta, Taipei and Seoul. It was discovered that ground surface temperatures substantially increased during the last century, much more than could be inferred by analytical inversion from logs in rural surroundings. Repeated measurements in some boreholes were carried

*Correspondence to: Peter Bayer, ETH Zurich, Department of Earth Sciences, Sonneggstrasse 5, 8092 Zurich, Switzerland
E-mail: bayer@erdw.ethz.ch

out by Hamamoto *et al*. (2008) to inspect the stability of the temperature logs. Instability at greater depths (without seasonal influence) was considered to be an indicator in variability of groundwater flow velocity. Perturbation of the logs by horizontal and vertical advective heat flow was assumed to be the reason that unrealistic surface cooling was inferred for the time before 1900, because their forward model assumes vertical conduction only.

Plenty of previous studies to analyse borehole logs and subsurface heat transport are based on the assumption that conduction is the dominant factor (e.g. Pollack *et al*., 1998; Beltrami *et al*. 2006). Although, the assumption of one-dimensional vertical heat conduction might not be suitable in mixed, conduction–advection controlled systems (Bense and Beltrami, 2007), which are characteristic in the presence of groundwater. For instance, downward groundwater flow might change temperature profiles into a shape that looks similar to the one caused by surface warming, and the initial and boundary conditions are not always linear (Kurylyk and MacQuarrie, 2013). Accordingly, for subsurface UHIs, the applicability of analytical reconstruction methods established in borehole climatology is restricted. The early works by Suzuki (1960) and Stallman (1963) provide solutions for solving one-dimensional conduction–advection equations, which can be used to estimate the vertical groundwater flow rate, but require a given surface temperature distribution. Even though both vertical and/or horizontal advection components and surface temperature changes can be included in analytical solutions (Domenico and Palciauskas, 1973; Lu and Ge, 1996; Kurylyk and MacQuarrie, 2013), limitations remain, for instance, typical layering of aquifers and thermal dispersion are neglected. Furthermore, for many cities, deep boreholes are typically rather scarce. This limits monitoring of continuous temperature profiles down to the undisturbed geothermal gradient. Alternatively, a numerical modelling framework may be adopted (Ferguson and Woodbury 2004; Epting *et al*. 2013). Although a numerical model can be more flexible and accurate, this comes at the expense of an enormous data requirement. Ideally, the selected numerical approach finds a compromise between data requirements and accuracy, which is intended in our study. Ferguson and Woodbury (2004), for example, set up generic 2D numerical models to simulate the effect of horizontal groundwater flow on the long-term development of a heat anomaly beneath single and multiple neighbouring buildings. Their study is oriented at the conditions representative for the city of Winnipeg, with a minor groundwater flow velocity of $4.0 \times 10^{-7}\,\mathrm{m\,s^{-1}}$ ($0.03\,\mathrm{m\,day^{-1}}$) in the simulated carbonate aquifer layer. Groundwater flow is shown to have only a minimal effect on the evolution of bulb-shaped thermal anomalies evolving in the modelled vertical cross sections.

The main objective of our work is to understand the interplay of conductive and advective forces during the evolution of a subsurface UHI, and especially to explore the role of regional horizontal groundwater flowing at much higher groundwater flow velocities than studied by Ferguson and Woodbury (2004). We focus on the city of Cologne, Germany where repeated measurements in the shallow groundwater revealed elevated temperatures by more than 5 K (Zhu *et al*., 2010; Menberg *et al*., 2013a). Little is known about the long-term effects that lead to the extensive subsurface UHI reaching a depth of more than 100 m. The currently available information is insufficient for a detailed numerical study including all natural and anthropogenic urban heat sources. Instead, here, a realistic scenario is studied by considering potential long-term trends of increased ground temperatures, which are implemented into a site-specific, simplified numerical model.

METHODOLOGY

In the following, first, the case study of Cologne is introduced, and the data survey and measurements in the study area are described. Then, a three-dimensional (3D) groundwater flow model is developed to capture the regional hydrogeological conditions. On the basis of this groundwater flow model, a vertical cross-section was chosen for a two-dimensional (2D) flow and heat transport model. We examine different scenarios with variable assumptions for elevated ground temperatures, recharge rates and advective–dispersive effects from horizontal groundwater flow. By comparison of simulated to measured groundwater temperature-depth (GWTD) profiles, the main factors that influence subsurface UHI heat transport are elucidated.

DATA COLLECTION

Data survey

This case study is conducted in the city of Cologne, where the climatic, such as past air temperatures (Figure 1), geological and hydrogeological information was collected.

The city lies on the Rhine River. It is one of the largest cities in Germany, with a population of around one million. We focus on the main city part, which is located on the western side of the Rhine. The study area is depicted in Figure 2, which also illustrates the subsequent model implementation.

The mean annual air temperature back in 1900, when the city in Cologne started growing fast, is about 8.7 °C (Figure 1). Because no earlier air temperature measurements are available for Cologne, we added data from 1900 to 1945 recorded in Aachen (DWD, 2010), which is only 70 km away. Linear regression for the whole period since 1900 reveals a mean linear increase of around 0.03 °C per year. The average regional annual precipitation from 1961 to

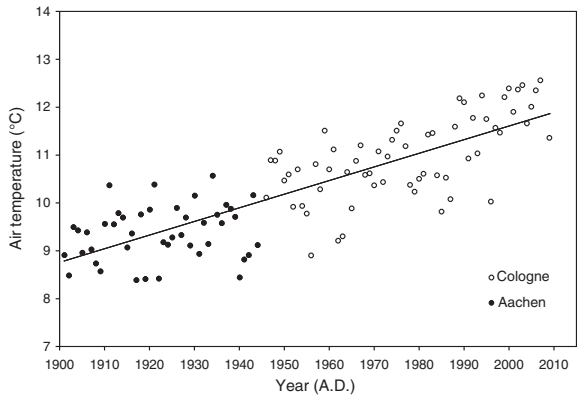

Figure 1. Mean annual air temperature recorded from 1900 to 2010 by a weather station in Stammheim in the northeastern part of Cologne, and by a weather station in Aachen (DWD, 2010)

1990 was around 774 mm (DWD, 2006). Groundwater recharge in Germany is commonly only about 16% of the precipitation (BGR, 2008) and is mainly concentrated in the winter period, when vegetation is least active.

Cologne is underlain by Quaternary terrace deposits that host a shallow aquifer with a thickness of around 20 m (Klostermann, 1992), and the major components of the urban aquifer are sands and gravels (Losen, 1984). The underlying aquitard consists of clays, silts, lignite and soft coals mixed in with thin sandy layers reaching to a depth of about 200 m (Balke, 1973; Hilden, 1988). The horizontal groundwater flow velocity in the aquifer is around 1 m day^{-1} (Balke, 1973). The groundwater flows towards the northeast and discharges into the Rhine River.

Field measurements

In three measurement campaigns in October 2009, September 2012 and December 2012, groundwater levels were measured. In 2009, data from 72 wells in the city, suburban and surrounding rural area were collected (Zhu *et al.*, 2010). Out of these, there are 46 wells located within the study area (Figure 2). In 2012, the piezometer levels of 15 wells were repeatedly recorded in the city. The measurements indicate that the water table is relatively stable in most of the wells distant from the river, but in the northeastern part near the river, the water levels vary by more than 1 m (data not shown). Despite this local and temporal variability, however, the derived main groundwater flow direction is always from west towards east with a calculated hydraulic gradient ranging between 5×10^{-4} and 7×10^{-4}, and no river infiltrating conditions are observed in the study area.

In the present work, we focus on the groundwater temperature data as reported by Zhu *et al.* (2010). GWTD profiles at 1 m intervals were recorded using SEBA KLL-T logging equipment. Well diameters range from 2 to 5 in (0.05–0.127 m), and the wells reach depths between 20 and 44 m. The positions of these wells are spatially distributed and associated with different types of land use, including built environment, green spaces and agricultural area. From the inspected 46 wells, ten wells (Figure 2) with characteristic GWTD profiles (Figure 3) for undisturbed agricultural area (wells 1, 2), green spaces (3, 4) and built environment in the city (5–10) are chosen as representatives to examine the conditions for different land-use types.

In agricultural areas, the measured GWTD profiles typically are smooth and not very variable. The measured temperature is around 1 °C below the current mean annual air temperatures in the city area (Figure 1). The closer the GWTD measurements are located to the city centre, generally, the higher the observed temperatures are, and the profiles tend to be less uniform. This reflects the growing number and superpositioning of anthropogenic heat sources, such as buildings and paved ground (Ferguson and Woodbury 2004, Menberg *et al.*, 2013a, b). Built-up areas commonly are associated with highest temperatures, reaching more than 16 °C in the city centre. Lateral heat transport from these sources apparently generates slightly higher temperatures beneath the city green spaces than found in remote rural regions.

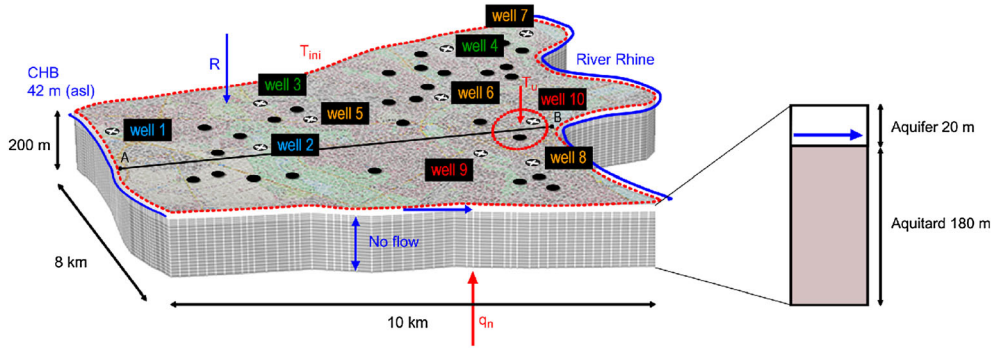

Figure 2. Three-dimensional conceptual model of the case study of Cologne including hydraulic and thermal boundary conditions, observation wells and a simplified vertical hydrogeological profile (CHB, constant head boundary; R, groundwater recharge; T_{ini}, initial temperature; T_u, urban temperature; q_n, natural geothermal heat flux). Cross-section A–B indicates the studied two-dimensional flow and heat transport model

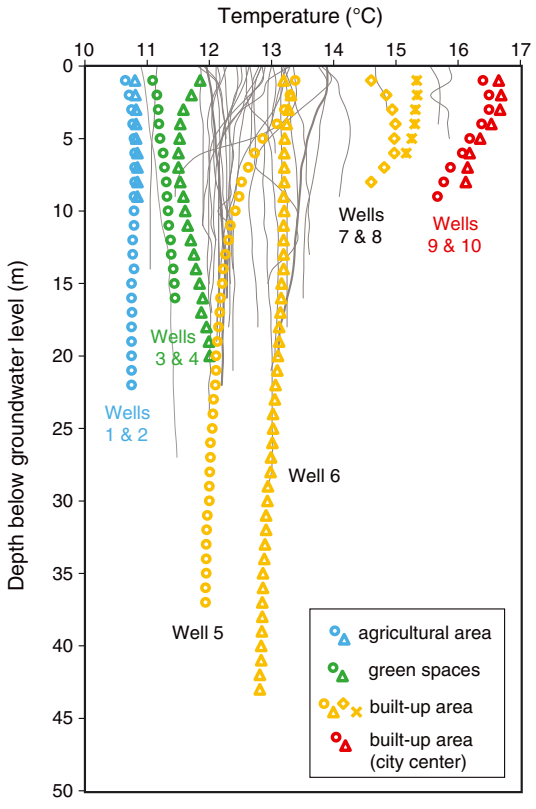

Figure 3. Measured groundwater temperature-depth profiles in Cologne. From the 46 profiles, those from wells 1–10 are selected as representatives for specific urban environments and examined further in Figure 11

REGIONAL 3D GROUNDWATER FLOW MODEL

A 3D numerical groundwater flow model that delineates the major hydraulic conditions of the shallow aquifer system was set up with FEFLOW (Version 6.0, Diersch, 2009), a finite element groundwater flow and transport simulator. The modelled area comprises 120.14 km^2 (Figure 2). It covers the main city area on the western side of the Rhine and part of the surrounding suburban areas. The numerical model consists of 40 layers, is about 200 m thick and has a total of around 260 000 nodes. The upper 20 layers, each with a thickness of 1 m, represent the main aquifer followed by 20 layers with variable thicknesses from 2 to 10 m corresponding to the aquitard in the succeeding texts. The aquifer is unconfined, and steady-state hydraulic conditions are simulated. The high resolution of the aquifer is chosen to characterize small-scale vertical temperature variabilities, with steepest thermal gradients expected in the upper part of the model. To limit the computational effort, the vertical grid size in the aquitard increases with depth.

Boundary conditions of the model are obtained from the groundwater level contour map and river head provided by the local water association (Erftverband, 1995). The boundaries at the north and south are oriented perpendicular to the reported groundwater head contours, and hence no flow boundaries are assigned (Figure 2). The western boundary is chosen by the mean groundwater head isoline of 42 m above sea level in the contour map, which is far beyond the built urban area. The Rhine River is represented in the model as an eastern head-dependent boundary. The water table, i.e. the upper boundary of the alluvial aquifer, is simulated as a free-surface boundary. Groundwater recharge, which in urban space is not generally well known because of surface sealing, was subsequently determined by model calibration.

To obtain a representative model setting, first, ranges of uncertain hydraulic model parameters are investigated, which are listed in Table I. These ranges guide automatic calibration of the model described in the results section. Further details on data sources and calibration procedures are given in the Supporting Information.

FLOW AND HEAT TRANSPORT SIMULATION

We chose steady state to approximate the long-term mean of recurrent and periodic conditions in the flow regime, while keeping the modelling effort on a reasonable level. However, urban groundwater temperatures are expected to follow long-term trends, and thus transient conditions are favoured in the subsequent coupled 2D flow and heat transport model.

The values of the thermal properties are chosen on the basis of previous studies in the Cologne area (Balke, 1977) and further literature sources (Gelhar *et al.*, 1992; VDI-4640/1, 2000; Maier and Grathwohl, 2006) (Table I). To eliminate the vertical influence of seasonal temperature fluctuation, the groundwater level, which is around 10–12 m below the surface, is taken as the top boundary for the heat transport simulation. The simulation starts in the year 1900 with an initial temperature at the top boundary of $T_{ini} = 8.7$ °C according to measured mean air temperature in the region (Figure 1). The upward geothermal heat flux value in Cologne region of $q_N = 59\ mW\ m^{-2}$ (Balke, 1977) is expressed by a constant flux boundary at the bottom of the model (Figure 2). Unspecified heat boundaries are assigned to the sides, with the river at the east having the same initial temperature as in the atmosphere (8.7 °C). The initial undisturbed temperature distribution is obtained by running the model for a burn-in phase of 10^8 days. Within this period, the model reaches quasi-steady-state conditions, with a maximum temperature change of less than 10^{-5} K within 100 years.

The developed model describes undisturbed thermal conditions. By selecting such settings for 1900, we presume that more than one century ago, main potential anthropogenic heat sources were absent. This is a crucial

Table I. Reported value ranges, selected and calibrated model parameter values for the 3D groundwater flow and 2D heat transport model

Parameter	Value range	Model input	Calibrated (this study)	References
Hydraulic conductivity of aquifer ($m\,s^{-1}$)	8.0×10^{-4}–7.0×10^{-3}		3.0×10^{-3}	Voigt and Kilian (2007)
Hydraulic conductivity of aquitard ($m\,s^{-1}$)	1.0×10^{-8}–1.0×10^{-6}		1.6×10^{-7}	Freeze and Cherry (1979)
Groundwater recharge ($mm\,a^{-1}$)	39 – 237		67.2	Erftverband (1995) DWD (2006)
Porosity of aquifer (−)	0.15–0.25	0.2		Balke (1973)
Porosity of aquitard (−)	0.14–0.57	0.3		McWhorter and Sunada (1977)
Thermal conductivity of porous media in aquifer ($W\,m^{-1}\,K^{-1}$)	1.7–5.0	2.1*		VDI-4640/1 (2000)
Thermal conductivity of aquitard ($W\,m^{-1}\,K^{-1}$)	1.1–5.1	1.9*		VDI-4640/1 (2000)
Water thermal conductivity ($W\,m^{-1}\,K^{-1}$)		0.6		VDI-4640/1 (2000)
Volumetric heat capacity of minerals ($MJ\,m^{-3}\,K^{-1}$)	2.1–2.4	2.2		VDI-4640/1 (2000)
Water heat capacity ($MJ\,m^{-3}\,K^{-1}$)		4.2		VDI-4640/1 (2000)
Longitudinal dispersivity (m)	5–20	10		Gelhar *et al.* (1992)
Transverse dispersivity (m)	0.05–1.0	0.03		Maier and Grathwohl (2006)

*Please note that FEFLOW input values for thermal conductivity of aquifer and aquitard, 2.1 and 1.9 $W\,m^{-1}\,K^{-1}$, refer to the arithmetic mean of solids and water saturated pore space. The corresponding geometric mean values are therefore 2.3 and 2.2 $W\,m^{-1}\,K^{-1}$, respectively.

assumption, and Ferguson and Woodbury (2004) already emphasized in their study on heat loss of buildings that time of construction plays an important role for the development of the heat anomaly. Although, it is hard to pinpoint the exact starting time of subsurface warming in Cologne, a large amount of heat flowing into the underground since the beginning of last century can be expected. However, little is known about the temporal temperature trends. Hence, various scenarios of increasing temperatures at the top are investigated, including background temperature rise (linear increase as air temperature in Figure 1), linear and step increase from 1900, 1955 and 1975 (Figure 4). The total simulation time is set to 110 years, from 1900 to 2010. Among the studied scenarios, linear increase from 1900 (8.7 °C) to 2010 (15 °C, measured in the groundwater in the city centre of Cologne) is considered as the urban reference case. Although this linear increase is the most straightforward option, we might also expect much more dynamic evolution of thermal inputs in the ground. As alternatives, step functions are defined, which, for example, could reflect the instantaneous effect of heat loss from additional new buildings. Comparison between the simulated results for these different trends will facilitate to judge their sensitivities.

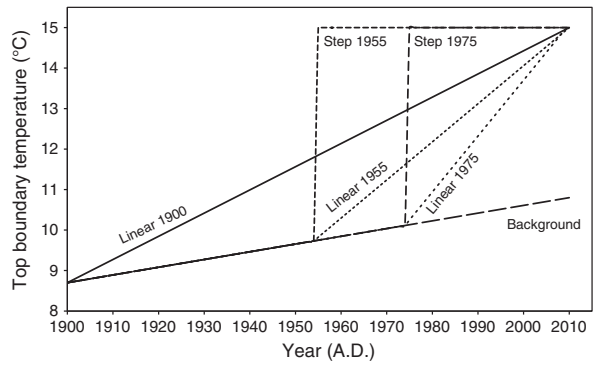

Figure 4. Scenarios of transient temperature boundary conditions (from 1900 to 2010) applied to control groundwater temperature at hot spot of the model

Detailed simulations of spatial development of potential heat sources over time as a consequence of city growth are beyond the scope of this study. Instead, an idealized hot spot of fixed size is initially defined, which represents the city centre. It encompasses a circular area with 1 km diameter, where the effects of the different transient top boundaries are assessed. The hot spot can be interpreted as a cutout of the city, an urban district with elevated temperature, which is separately examined. This means, potential lateral interaction, such as different adjacent heat sources, or large scale expansion of the area of increased ground heat flux, is not currently accounted for in the model. This aspect is discussed consequently with the modelling results.

At the hot spot, we are primarily interested in the evolution of the induced thermal anomaly in the vertical and groundwater flow direction (along A–B, Figures 2 and 5), and thus specifically inspect the cross-section through the centre (Figure 2). To simplify the model and shorten simulation time, for this cross-section A–B, an equivalent 2D vertical steady-state flow and transient heat transport model is constructed and validated with the 3D model (see Supporting Information). Analogous to the 3D model, the hydraulic boundary on the western side (A) of

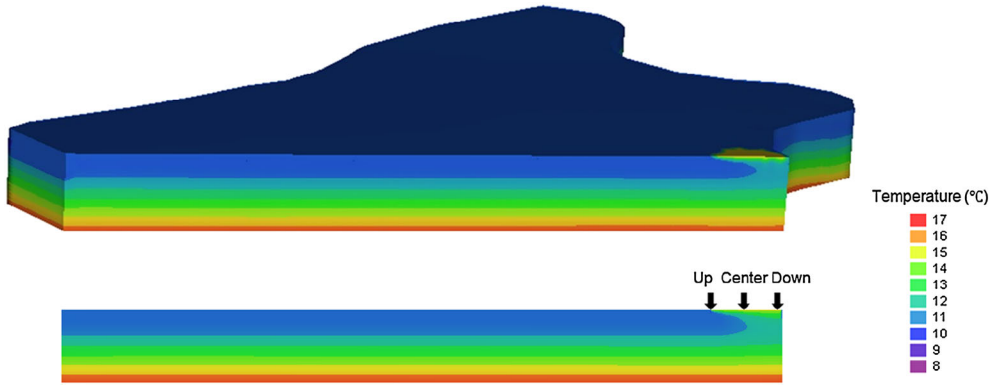

Figure 5. Temperature distribution after 110 years simulation (reference case with linear temperature increase at hot spot) for selected cross-section of 3D model and of emulated vertical 2D model; 'center' indicates the city centre and 'down' is near river Rhine

the 2D model is a constant head of 42 m, and on the eastern side (B), the depth of the river is 20 m, with a head of 36.5 m. The 2D model has a length of 10 km and a thickness of 200 m. Same spin-up simulation was applied, and results show the same initial vertical temperature distribution as the 3D model. To emulate the hot spot, different increasing temperature scenarios were assigned at the top boundary of the 2D model, from 9 km to 10 km.

In the following presentation of the results, first, the focus is set on the sensitivity of some potentially crucial model parameters. The impact of recharge and thermal dispersion is discussed under undisturbed condition and with hot spots. In addition, the influences of different temperature top boundaries and hot spot size are examined. The model results are juxtaposed to measured GWTD profiles to inspect the relevance of flow conditions and local hot spots of temperature profiles for the Cologne underground.

Table II. Flow balance of the 3D groundwater flow model of Cologne

	Inflow ($10^3\,m^3\,day^{-1}$)	Outflow ($10^3\,m^3\,day^{-1}$)
Constant head boundary in the west	81.33	—
Groundwater recharge	19.65	—
Sum of constant head boundary in the west and groundwater recharge	100.98	—
River boundary in the east	—	101.00

RESULTS AND DISCUSSION

Influence of groundwater recharge on heat transport

The values of hydraulic conductivities (aquifer, $3.0\times10^{-3}\,m\,s^{-1}$; aquitard, $1.6\times10^{-7}\,m\,s^{-1}$) and recharge rate ($67.2\,mm\,a^{-1}$) of the 3D flow model are adjusted within the given ranges by hydraulic head calibration (see Supporting Information) with support of the parameter estimation software PEST (Version 12, Doherty, 2010). The resulting water flow balance of the 3D groundwater flow model is provided in Table II.

The automatic calibration reveals that the inversion problem is not well posed, and a range of parameter value combinations produces equally satisfactorily predictions. The best fit is obtained with $67.2\,mm\,a^{-1}$ (Table I), although several other close-optimal solutions exist. The essential question here is how sensitive this model specification and especially the recharge value is for the simulated results. Several previous studies indicated that vertical groundwater fluxes can cause temperature anomalies, and that in recharge areas, geothermal gradients are smaller (e.g. Domenico and Palciauskas, 1973; Taniguchi *et al.*, 2003; Ferguson *et al.*, 2006). Furthermore, groundwater recharge can accelerate shallow subsurface warming (Kurylyk and MacQuarrie, 2013).

Because around 70% of the study area is highly urbanized with sealed concrete surfaces and drainage systems, it is reasonable to expect such a small local effective recharge rate. Trial simulations with and without recharge resulted in negligible differences in subsurface temperatures (not shown here). Under steady-state conditions and for constant surface temperature (i.e. initial undisturbed temperature distribution), the simulated GWTD profiles with recharge result in minor differences (<1% relative discrepancy) compared with the ones with no recharge (data not shown). This is because the horizontal groundwater flow rate is around three orders of magnitude higher than the recharge. A similar outcome was observed, for instance by Molina-Giraldo *et al.* (2011b), who could demonstrate the minor impact of groundwater recharge (using $300\,mm\,a^{-1}$) for their heat transport model of a river infiltrating in an aquifer.

If we ignore the groundwater recharge at the top boundary in the model of the reference case, the

temperature beneath the centre of the hot spot only decreases by an average of 0.03 K along the first 50 m depth (results not visualized). Nevertheless, in densely populated urban areas with high air and ground temperatures and higher groundwater recharges, more anthropogenic heat might also penetrate into the ground and locally pronounced advective heat transport by recharge has to be considered more carefully. Foulquier *et al.* (2009), for example, observed that the thermal amplitude of groundwater can be increased dramatically by stormwater infiltration at seasonal and event scales.

In conclusion, groundwater recharge rates obtained by fitting the numerical model are less than 100 mm a^{-1} in Cologne, and thus do not contribute much to shallow subsurface warming in this city. If we assume an increase of surface temperatures by 4 K, the average heat transfer to the aquifer by recharge in a period of 100 years is about 1.1×10^{11} kJ km^{-2}, whereas, by heat conduction, it is more than fivefold (5.8×10^{11} kJ km^{-2}). In contrast, local anthropogenic heat sources, such as leakage of sewage or water distribution networks, might play a more prominent role (e.g. Menberg *et al.*, 2013b). This is reported for cities in England. For example, the study by Lerner (1990) showed that urbanization reduces the groundwater recharge, but creates new and additional sources for recharge, such as leaking from water mains and sewers.

Influence of groundwater flow for undisturbed conditions

Vertical and horizontal groundwater flow. At the study site, a shallow aquifer with substantial groundwater flow velocity (v) of around 1 m day^{-1} exists, and, in comparison with the study by Ferguson and Woodbury (2004), horizontal advection is therefore expected to play an important role for the evolution of the groundwater temperatures. Lu and Ge (1996) demonstrated that when the horizontal heat and fluid flow is greater than 30% of the vertical one, it has a significant effect on the vertical temperature distribution. Ferguson *et al.* (2006) concluded that when the downward Darcy flux is smaller than 2.0×10^{-8} m s^{-1} (0.63 m a^{-1}), it does not significantly change the temperature profile under steady-state thermal conditions. In our study area, which is in a river valley, the dominant flow direction in the urban aquifers is horizontal, with significant flow rates of about 1 m day^{-1} (365 m a^{-1}); whereas the vertical groundwater flux due to recharge is only around 1.9×10^{-4} m day^{-1} (0.07 m a^{-1}). Simulation results show that consistent with the criterion set by Ferguson *et al.* (2006), it only has a minor influence on the temperature profile with a temperature change <0.03 K.

Influence of transverse thermal dispersion. A mechanism, which has not been studied in this context, is the impact of the transverse thermal dispersion on vertical temperature gradients. Thermal dispersion comprises heat conductivity and hydromechanical dispersion in groundwater. Mechanical dispersion in porous media is caused by the movement of a heat carrying fluid, such as groundwater. The different flow pathways on the pore scale create differential advection, and the mixing of the pore-scale interstitial water causes spreading of the temperature gradients. Macroscopic scale heterogeneity of a permeability field also contributes additionally to dispersion, and increases uncertainty of the spreading of heat plumes (e.g. Molina-Giraldo *et al.*, 2011a). Finally, heat conduction in water and solids contributes to the overall dispersion in heat transport in groundwater (e.g. Bons *et al.*, 2013).

In our high-velocity case, transverse dispersion can be expected to influence the vertical heat flow and the GWTD profile. The value of the hydromechanical transverse dispersivity, however, is not exactly known and has not been examined for the Cologne area. In general, there are only few studies specifically dedicated to experimental or model-based estimations of thermal transverse and longitudinal dispersivities (e.g. Molina-Giraldo *et al.*, 2011a; Rau *et al.*, 2012; Bons *et al.*, 2013; Stauffer *et al.*, 2013). Hence, in our reference case, we initially approximate the field-scale hydrodynamic transverse dispersivity by Maier and Grathwohl (2006) with $\alpha_t = 0.03$ m, which was derived for a sand and gravel aquifer in south-west Germany. This field-scale derived (fitted) transverse dispersivity is therefore a bulk parameter, which also accounts for possible effects of heterogeneity or non-stationarity. The chosen value is at the lower range of reported field-scale transverse dispersivities applied in field experiments and modelling studies ranging between 0.005 and 10 m (Stauffer *et al.*, 2013). Hence, even higher values might occur in more heterogeneous environments. In contrast, typically, laboratory-scale (local-scale) derived transverse dispersivities are much smaller ($\alpha_t < 1.8 \times 10^{-4}$ m; e.g. Olsson and Grathwohl, 2007; Bauer *et al.*, 2009). Furthermore, the transverse dispersivity may depend slightly on the flow velocity of the studied system (e.g. Chiogna *et al.* 2010). The latter however is not known for the studied aquifer; thus here, only a range of transverse dispersivities is examined in more detail.

Groundwater temperature-depth profiles simulated for undisturbed conditions are compared for different transverse dispersivities ($\alpha_t = 0$, 0.03, 0.1 and 1 m). With increase of dispersivity, the simulated vertical temperature gradient along the aquifer becomes smaller in the aquifer because of the increase in vertical mixing (Figure 6). This is a similar effect as that from vertical groundwater flow, such as described, for example, by Taniguchi *et al.* (2003). Thus, macroscale mechanical dispersion reveals to be an important process for the heat transport in vertical direction. The hydromechanical dispersion coefficients ($D_t = v \times \alpha_t$) and

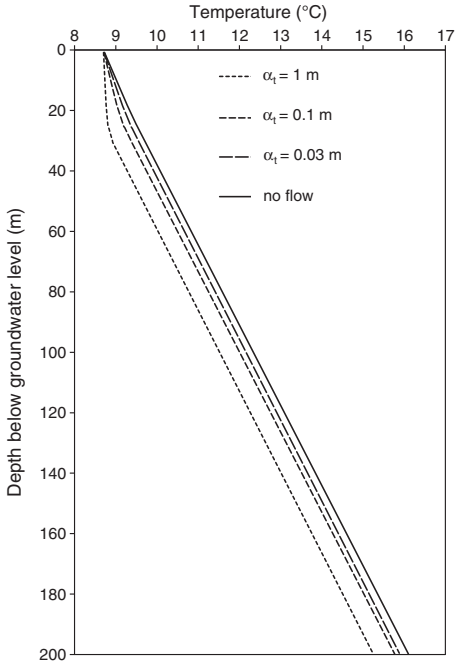

Figure 6. Simulated initial undisturbed groundwater temperature-depth profiles (without hot spot) under conduction-dominated condition (solid line) and flow conditions with different transverse dispersivity (α_t) values; groundwater recharge is 67.2 mm a^{-1} in each scenario

thermal diffusivities ($\kappa = \lambda/C_v$, λ and C_v are thermal conductivity and volumetric heat capacity of the aquifer) can be used to quantitatively compare the influence of dispersion and conduction. For a horizontal flow velocity of 1 m day^{-1}, if α_t equals to 0.1 m, the calculated value of D_t (1.2×10^{-6} m^2 s^{-1}) is already larger than κ (8.8×10^{-7} m^2 s^{-1}). When $\alpha_t \geq 1$ m, dispersion becomes even more dominant and complete mixing of the aquifer happens (Figure 6).

Influence of groundwater flow with local heat sources

Different temperature top boundaries. As illustrated in Figure 6, the effect of horizontal groundwater flow under steady-state thermal conditions on ground temperature evolution depends on the degree of transverse dispersion, and the influence is more evident when dispersivities are larger than 0.1 m. Figure 7 shows simulated GWTD profiles at different locations (upstream, centre and downstream) of the hot spot, given transient conditions with different top boundary temperature increasing scenarios (Figure 4). The dispersivity is not varied here and set to the default value of $\alpha_t = 0.03$ m. The simulated profiles are comparable in the upper part, down to the aquifer basis at 20 m, as well as in a depth of more than 100 m below the water table. Even if slightly increased temperatures are simulated at greater depth than 100 m, all curves converge to a linear trend representing undisturbed conditions. Because of horizontal groundwater flow, all the simulated profiles at upstream are almost the same (Figure 7a), and at centre and downstream, the differences become larger.

As expected, temperature increasing scenarios with earlier onset of the hot spot generate deeper penetration, and for the different linear trends, the scenario starting from 1900 ('Linear 1900' in Figure 7c) generates a more pronounced anomaly than the scenario initiated in 1955 ('Linear 1955' in Figure 7c). Because of thermal diffusion and dispersion, step functions assigned to the top boundary also induce smooth profiles. Temperatures are higher for stepwise than linear increase starting from the

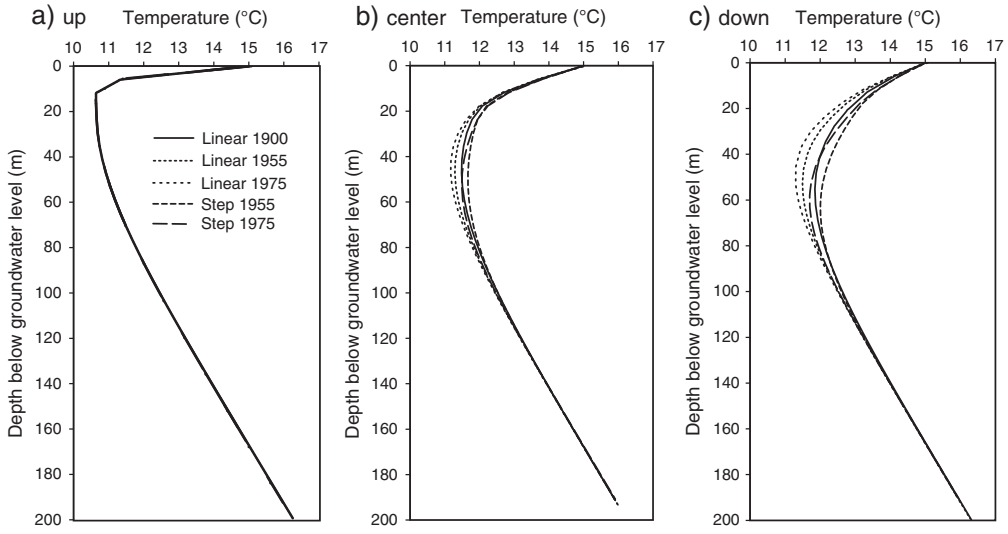

Figure 7. Simulated groundwater temperature-depth profiles at different locations (upstream, centre and downstream) of hot spot assuming no groundwater flow and horizontal flow with different transverse dispersivity (α_t) values

same point in time (e.g. the scenario 'Step 1955' shows higher temperatures than 'Linear 1955' in Figures 7b and 7c), and this can be easily explained by the higher average temperature at the top boundary for this scenario and thus a higher amount of heat introduced to the subsurface. In all profiles, because of horizontal groundwater flow, the influence of different increasing temperature top boundaries is only marginal in the shallow parts (<20 m depth).

Transverse dispersion effects at different locations. The simulated profiles show that the footprint of elevated urban heat flux can be tracked to a maximum of about 100 m, which is similar to the deviation depth observed in other cities, such as Winnipeg with a depth of ~130 m (Ferguson and Woodbury, 2004) and Tokyo with a depth of 140 m (Taniguchi *et al.*, 2007). The different trends of past temperature increase obviously do not have substantial impact on the shallow part of temperature profiles, given that the initial ($T_u = 8.7$ °C) and final ($T_u = 15$ °C) conditions are known. Thus, in the following, we stick to the linear increase from 1900 (urban reference case), and concentrate on the role of transverse dispersion. This is investigated by visualizing the thermal conditions beneath the hot spot, and by comparing the temperature profiles simulated at the central as well as upstream and downstream fringe position (Figures 8 and 9).

Figure 8 shows that horizontal groundwater flow in the shallow aquifer deviates from the thermal anomaly, evolving beneath the hot spot, in the downstream direction. This is also reflected in the vertical temperature profiles in Figure 9. In the upstream position (Figure 9a), horizontal flow therefore prevents the evolution of deeper temperature alterations. In comparison, for conduction-dominated conditions, simulated by switching off groundwater flow in the model, the thermal anomaly is not deviated, and vertical thermal diffusion is most effective. Still, despite the high flow velocity of 1 m day^{-1}, horizontal advection does not act as a thermal barrier. In downstream direction, conduction-induced profiles become similar to those conditions with small to moderate values of macroscale transverse dispersivity, which is $\alpha_t \leq 0.1$ m (Figure 9c).

Figures 8 and 9 illustrate that most pronounced effects occur for conditions with high transverse dispersion ($\alpha_t = 1$ m). This scenario could represent substantial macrodispersive effects as a consequence of aquifer heterogeneity. For simulating the aquifer of Cologne, we assume $\alpha_t = 0.03$ m, which, however, is highly uncertain and can not be validated here. In fact, the formation hosting the aquifer consists of terrace deposits with interbedding gravels and sands. These structures and heterogeneities are not currently resolved in our simplified model, which assumes homogeneous aquifer and aquitard layers. Hence, in the field, macrodispersion may play an even more prominent role than simulated by the presented models. Although, such

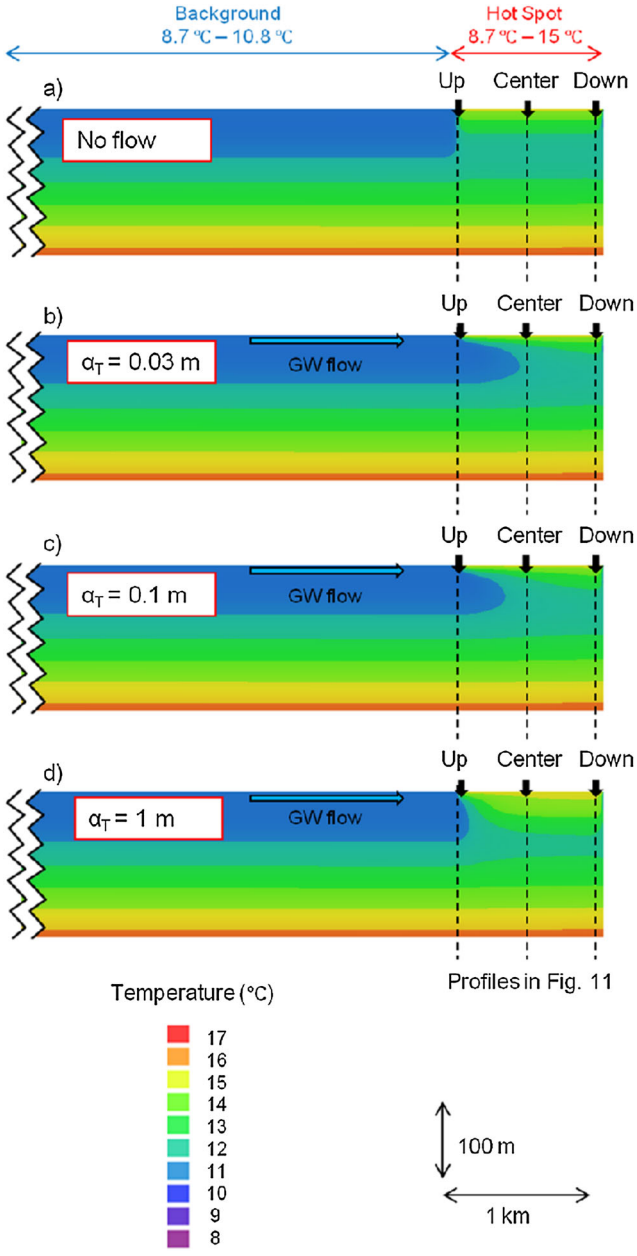

Figure 8. Simulated temperature distribution after 110 years (urban reference case, with 1 km hot spot) of vertical 2D models with different transverse dispersivity (α_t) values (b–d) and no horizontal groundwater flow (a). The groundwater flows from left to right with a velocity of about 1 m day^{-1}, and a cold plume develops below the hot spot. Temperature profiles at upstream, centre and downstream position of the hotspot of each scenario are compared and shown in Figure 9

systems using larger thermal transverse dispersivities ($\alpha_t > 1$ m) are rare (Stauffer *et al.*, 2013). For example, Smith and Chapman (1983) applied a thermal transverse dispersivity of 10 m in their 2D flow and transport model. However, they considered a sedimentary basin on kilometre scale (40 km wide and 5 km deep) and not an urban scale.

Because the temperature profiles at center, up or downstream locations are distinct, the excess heat stored

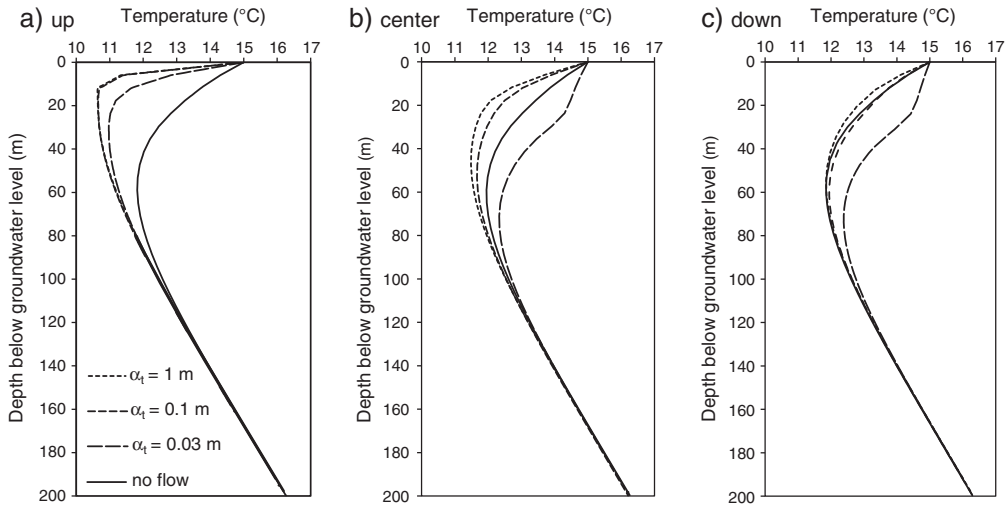

Figure 9. Simulated groundwater temperature-depth profiles with different transverse dispersivity (α_t) values at different locations (upstream, centre and downstream) beneath the hot spot (Figure 8). The dotted blue lines indicate the lower boundary of the aquifer. Additionally, the profile derived for no horizontal groundwater flow in the aquifer is shown

at such locations is also different. By heat content calculation for the reference case (Zhu *et al.* 2010), the total extra heat content at upstream, center and downstream are $Q_{up} = 3.62 \times 10^{10}$ kJ km^{-2}, $Q_{center} = 1.08 \times 10^{11}$ kJ km^{-2} and $Q_{down} = 1.53 \times 10^{11}$ kJ km^{-2}, respectively.

Size of hot spot. The hot spot scenario is based on the extension of the 15 °C temperature area on the groundwater temperature contour map (Zhu *et al.* 2010), and a size of 1 km is just an approximation of local conditions in the city of Cologne. In fact, the distribution of heat sources in the city is very heterogeneous, and thus, the superimposing heat sources could cover a larger area. If, for example, we extend the hot spot to 3 km, the simulated temperature profile in the upstream is the same as for the 1 km case, but the profiles at the centre and downstream show higher temperatures for 3 km (Figure 10). However, for the case studied here, the difference between the 3 km centre and downstream profiles is only minor, which indicates that the size of the hot spot has a limited influence until 1.5 km from the upstream, and after this distance, the impact of cold groundwater plume coming from upstream almost vanishes.

Comparison between simulated and measured temperature-depth profiles

During the 2009 field campaign, GWTD profiles were recorded at 46 wells in the study area. Because of spatial variation in land-use type, differences in heating history, the local presence of different heat sources and hydrogeological influences, temperature profiles in the city show pronounced spatial variability. Here, ten wells with characteristic temperature profiles covering all different land-use types and the measured temperature ranges are chosen (Figure 2).

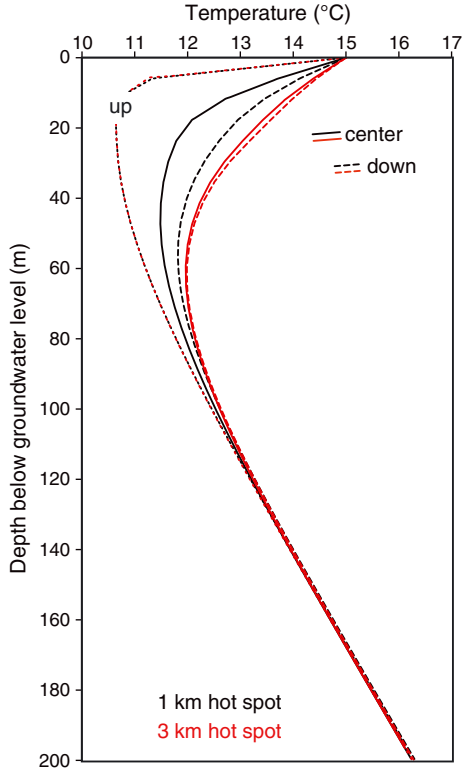

Figure 10. Comparison of simulated groundwater temperature-depth profiles at different locations (upstream, centre and downstream) with 1 and 3 km hot spot, respectively

The numerical model is used to reproduce these profiles to identify governing factors and to study, in general, the consistency of our modelling approach. Simulated profiles are compared separately for the measured profiles at given land use types. Again, a hot spot of 1 km extension

is implemented. In the four simulated temperature variants (10.8 °C, 13.5 °C, 15 °C and 17 °C), a standard linear trend since 1900 is assumed with the final temperature at the hot spot oriented at average values characteristic for different land-use types. These are 10.8 °C in 2010 for undisturbed conditions, 13.5 °C and 15 °C for built envorinment and 17 °C as observed in the highly urbanized city centre.

Undisturbed conditions are found in measurements in the surrounding rural area of Cologne: Wells 1 and 2 are located in agricultural land, and the vertical measured GWTD profiles are very similar with a nearly constant temperature of 10.8 °C. The measured profiles at these wells are reproduced by the model, which shows that the model is accurately calibrated to these undisturbed conditions. The measured temperature in urban green spaces is about 1 °C

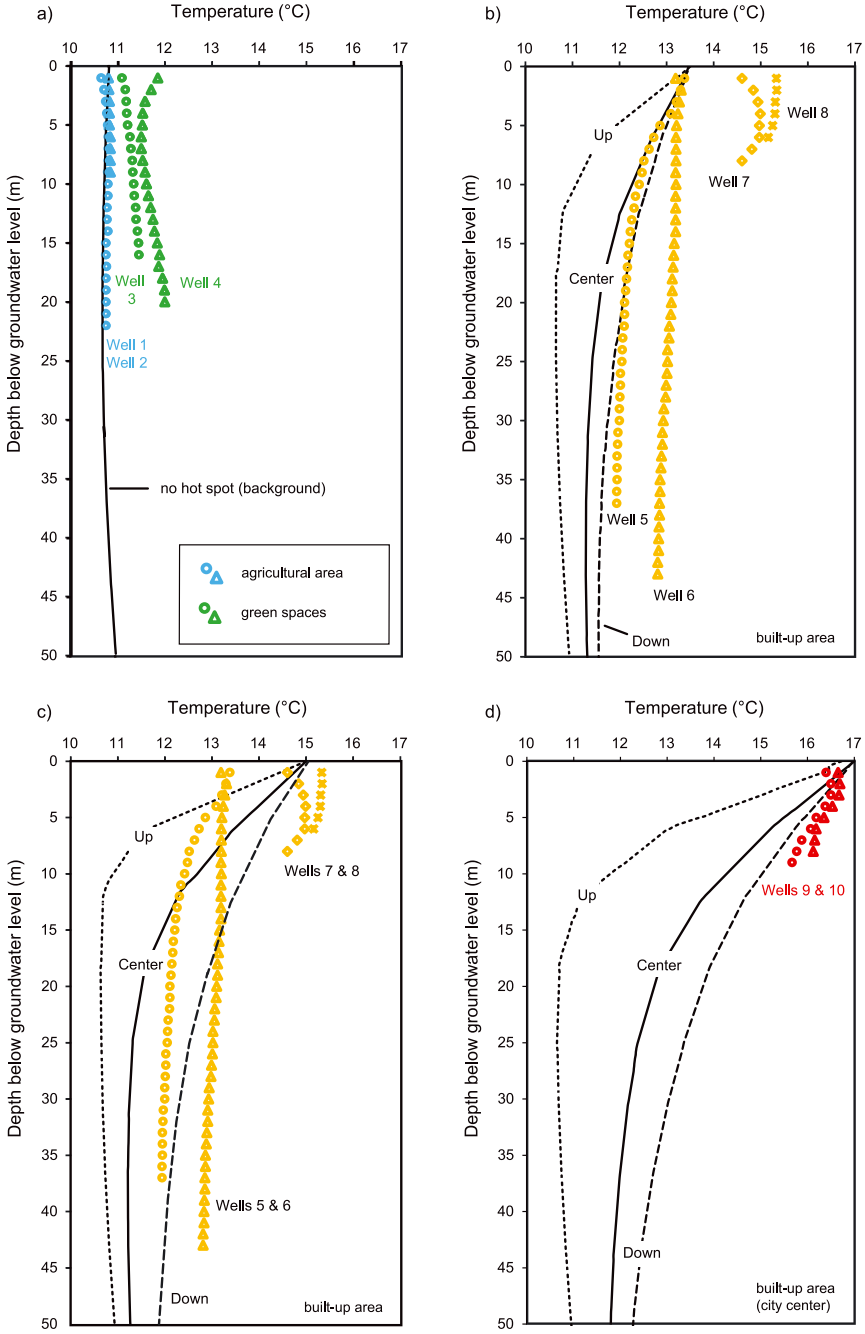

Figure 11. Simulated and measured groundwater temperature-depth profiles from different land-use types in Cologne (Figure 3)

higher than the simulated undisturbed temperature. When moving towards the city centre, measured groundwater temperatures increase and the temperature-depth profiles are perturbed, which is revealed to be specific for each well. When simulating the hot spot with different temperatures in 2010, the profiles that are found in upstream, centre or downstream position may fit in the uppermost, shallow profile, however, not in the deeper parts of the wells. Here, typically measured temperatures remain high and the profiles appear less inclined than the simulated ones (Figure 11b–d). On the basis of the previous analysis on crucial model configurations, we can identify several potential reasons for this discrepancy.

One principal reason is that the generic hot spot scenario is only an approximation of the site-specific and local conditions of the city of Cologne. The true heterogeneity of spatially and temporally variable features can hardly be resolved with our simplified scenarios. Comparison with measured profiles confirms that for a city, a much more extensive hot spot or, on fine resolution, multiple overlapping hot spots existing in the entire city area can be expected. Downstream of an area with elevated heat flux, groundwater temperature profiles tend to be more vertical as a consequence of transverse mixing. This also means that in this case, transverse dispersion may play an important or even dominant role. Alternatively, merely assuming more intense macrodispersion than specified in our reference model would lead to more realistic temperature profiles. This could be an indication that the role of subsurface heterogeneity is underestimated. Finally, an apparent reason for higher temperatures in the deeper wells is higher vertical heat fluxes in the past than estimated by the linear trend, which might date back before the year 1900, i.e. time zero in the current model.

CONCLUSIONS

During the past hundred years, because of urbanization, a large amount of anthropogenic heat has entered the subsurface of cities. The anthropogenic heat discharge elevated the temperature of a local urban aquifer beneath the city of Cologne, Germany, by up to more than 5 K. On the basis of simulation results from site-specific modelling, we can conclude that, for urban conditions such as in Cologne, average groundwater recharge rates are very low, and recharge does not play a significant role in urban groundwater temperature evolution. Because the dominant flow direction in the Cologne urban aquifers is horizontal, with significant flow rates, the influence of horizontal groundwater flow on subsurface temperature evolution has to be addressed.

It is shown that field-scale transverse dispersion causes additional vertical mixing and vertical heat flux, which perturbs GWTD profiles. The influence of this mechanism substantially depends on the effective transverse dispersivity and is more pronounced in more heterogeneous media, especially with local heat sources, than under undisturbed conditions. In the Cologne case, the chosen values of transverse dispersivities ranging between 0.03 m and 1 m are already more influential than vertical heat transport by groundwater recharge for both undisturbed conditions and hot spot scenarios. When α_t is larger than 1 m, instead of conduction, dispersion becomes the dominant process of vertical heat transport in the aquifer. Furthermore, our study shows that, under undisturbed conditions, the transverse dispersion could lead to a concave upward temperature distribution (Figure 9b and 9c), which could also be caused by downward groundwater flow. In urban regimes, exclusion of transverse dispersion in aquifers with high horizontal groundwater flow velocity, when analysing GWTD profiles, thus may result in erroneous estimates of surface warming rate or groundwater recharge.

When horizontal advection is the dominant heat transport process, a subsurface UHI might be moved downstream. Consequently, the GWTD profiles in urban aquifers are strongly influenced by the relative position and distance (upstream or downstream) to the anthropogenic heat sources, which were also demonstrated by Ferguson and Woodbury (2004). It is shown by numerical modelling that different increasing temperature trends and the size of the heat source (simulated as hot spot) also play a role on temperature evolution, especially at centre and downstream location, if distances are less than 1.5 km. Horizontal groundwater flow causes a cold plume below the city and heat discharge into the river. With an outflow rate of $1.0 \times 10^5\ m^3\ day^{-1}$ and a temperature gradient of 4 K, the amount of heat that is discharged to the river per year is about 6.1×10^{11} kJ.

The comparison of measured and simulated GWTD profiles also indicates that even in idealized scenarios, temperature profiles are rather complicated. They are hard to interpret and thus it is difficult to capture the driving subsurface heat transport mechanisms with streamlined scenarios. The heat flow in urban subsurface depends on many local and site-specific parameters, and a more detailed resolution of underground geological structures and the temporally variable heat urban sources would be desirable.

ACKNOWLEDGEMENTS

We would like to thank two anonymous reviewers for their fruitful comments. We also would like to acknowledge the assistance of Steffen Rehner during the field campaign in Cologne, and Valentin Wagner for technical support with the numerical simulation. Furthermore, we would like to thank the Erftverband and the RheinEnergie, particularly Stefan Simon and Stefan Schiffmann for providing data, as

well as assistance with the field measurements. This study was supported by the Federal Ministry for Education and Research (BMBF) scholarship programme for International Postgraduate Studies in Water Technologies (IPSWaT), by the Swiss National Science Foundation (SNSF) under grant number 200021L 144288, and the German Research Foundation (DFG), under grant number BL 1015/4-1.

REFERENCES

Balke K-D. 1973. Geothermische und hydrogeologische Untersuchungen in der südlichen Niederrheinischen Bucht. Bundesanstalt für Bodenforschung und den Geologischen Landesämtern der Bundesrepublik Deutschland, Hannover.

Balke K-D. 1977. Das Grundwasser als Energietraeger. *Brennstoff-Warme-Kraft* **29**: 191–194.

Bauer RD, Rolle M, Bauer S, Eberhardt C, Grathwohl P, Kolditz O, Meckenstock RU, Griebler C. 2009. Enhanced biodegradation by hydraulic heterogeneities in petroleum hydrocarbon plumes. *Journal of Contaminant Hydrology* **105**: 56–68. DOI: 10.1016/j.jconhyd.2008.11.004.

Beltrami H, Bourlon E, Kellman L, Gonzalez-Rouco JF. 2006. Spatial patterns of ground heat gain in the Northern Hemisphere. *Geophysical Research Letters* **33**(6). DOI: 10.1029/2005gl025676.

Bense V, Beltrami H. 2007. Impact of horizontal groundwater flow and localized deforestation on the development of shallow temperature anomalies. *Journal of Geophysical Research-Earth Surface* **112**(F4). DOI: 10.1029/2006jf000703.

BGR. 2008. Water water cycle/water balance for Germany. Available from: http://www.bgr.bund.de/EN/Themen/Wasser/Bilder/Was_wasser_startseite_wasserkreis_g_en.html. Federal Institute for Geosciences and Natural Resources.

Bodri L, Cermak V. 1997. Climate changes of the last two millennia inferred from borehole temperatures: results from the Czech Republic 2. *Global and Planetary Change* **14**(3-4): 163–173. DOI: 10.1016/S0921-8181(96)00010-0.

Bons PD, van Milligen BP, Blum P. 2013. A general unified expression for solute and heat dispersion in homogeneous media. *Water Resources Research* **49**(10): 6166–6178. DOI:10.1002/wrcr.20488.

Chiogna G, Eberhardt C, Cirpka OA, Grathwohl P, Rolle M. 2010. Evidence of compound-dependent hydrodynamic and mechanical transverse dispersion by multitracer laboratory experiments. *Environmental Science and Technology* **44**: 688–693. DOI: 10.1021/es9023964.

Doherty J. 2010. *PEST Model-Independent Parameter Estimation User Manual: 5th Edition*. Watermark Numerical Computing: Corinda, Australia.

Domenico PA, Palciauskas VV. 1973. Theoretical analysis of forced convective heat transfer in regional ground-water flow. *Geological Society of America Bulletin* **84**(12): 3803–3814. DOI: 10.1130/0016-7606.

DWD. 2006. Mittelwerte des Niederschlages, Deutscher Wetter Dienst.

DWD. 2010. Monatliche Temperaturwerte, Deutscher Wetter Dienst.

Erftverband. 1995. Basisplan III zur Sicherstellung der Wasserversorgung im Bereich des ErftverbandsRep., Erftverband, Bergheim.

Epting J, Händel F, Huggenberger P. 2013. Thermal management of an unconsolidated shallow urban groundwater body. *Hydrology and Earth System Sciences* **17**: 1851–1869. DOI: 10.5194/hess-17-1851-2013.

Ferguson G, Beltrami H, Woodbury AD. 2006. Perturbation of ground surface temperature reconstructions by groundwater flow? *Geophysical Research Letters* **33**(13). DOI: 10.1029/2006gl026634.

Ferguson G, Woodbury AD. 2004. Subsurface heat flow in an urban environment. *Journal of Geophysical Research-Solid Earth* **109**(B2). DOI: 10.1029/2003jb002715.

Ferguson G, Woodbury AD. 2007. Urban heat island in the subsurface. *Geophysical Research Letters* **34**(23). DOI: 10.1029/2007gl032324.

Foulquier A, Malard F, Barraud S, Gibert J. 2009. Thermal influence of urban groundwater recharge from stormwater infiltration basins. *Hydrological Processes* **23**(12): 1701–1713. DOI: 10.1002/hyp.7305.

Freeze RA, Cherry JA. 1979. *Groundwater*. Prentice-Hall: Englewood Cliffs, NJ, USA.

Gelhar LW, Welty C., Rehfeldt KR. 1992. A critical review of data on field-scale dispersion in aquifers. *Water Resources Reseatch* **28**(7): 1955–1974. DOI: 10.1029/92wr00607.

Gunawardhana L, Kazama S. 2011. Climate change impacts on groundwater temperature change in the Sendai plain, Japan. *Hydrological Processes* **25**: 2665–2678. DOI: 10.1002/hyp.8008.

Hamamoto H, Yamano M, Kamioka S, Nishijima J, Monyrath V, Goto S, Taniguchi M. 2008. Estimation of the past ground surface temperature change from borehole temperature data in the Bangkok area. In *From Headwaters to the Ocean*, Taniguchi M (ed). Taylor and Francis: Baton Rouge, FL, USA.

Hilden HD. 1988. Geolgie am Niederrhein. Geologisches Landesamt Nordrhein-Westfalen.

Huang SP., Pollack HN, Shen PY. 2000. Temperature trends ever the past five centuries reconstructed from borehole temperatures. *Nature* **403**(6771): 756–758. DOI: 10.1038/35001556.

Huang SP, Taniguchi M., Yamano M, Wang CH. 2009. Detecting urbanization effects on surface and subsurface thermal environment -- A case study of Osaka. *Science of the Total Environment* **407**(9): 3142–3152. DOI:10.1016/j.scitotenv.2008.04.019.

Klostermann J. 1992. Das Quartär der Niederrheinischen Bucht - Ablagerungen der letzten Eiszeit am Niederrhein. 4. Auflage, Krefeld. Geologisches Landesamt Nordrhein-Westfalen.

Kurylyk BL, MacQuarrie KTB. 2013. A new analytical solution for assessing climate change impacts on subsurface temperature. *Hydrological Processes*. DOI: 10.1002/hyp.9861.

Lerner DN. 1990. Groundwater recharge in urban areas. *Atmospheric Environment. Part B. Urban Atmosphere* **24**(1): 29–33. DOI: 10.1016/0957-1272(90)90006-G.

Losen H. 1984. Grundwasserstände und Grundwasserbeschaffenheit im südlichen Teil der linksrheinischen Kölner Scholle. Dissertation RWTH Aachen.

Lu N, Ge S. 1996. Effect of horizontal heat and fluid flow on the vertical temperature distribution in a semiconfining layer. *Water Resources Research* **32**(5): 1449–1453. DOI: 10.1029/95wr03095.

Maier U, Grathwohl P. 2006. Numerical experiments and field results on the size of steady state plumes. *Journal of Contaminant Hydrology* **85**(1–2): 33–52. DOI: 10.1016/j.jconhyd.2005.12.012.

McWhorter DB, Sunada DK. 1977. *Ground-Water Hydrology and Hydraulics*. Water Resour. Publications: Ft. Collins, CO, USA.

Menberg K, Bayer P, Zosseder K, Rumohr S, Blum P. 2013a. Subsurface urban heat islands in German cities. *Science of the Total Environment* **442**(0): 123–133. DOI: 10.1016/j.scitotenv.2012.10.043.

Menberg K, Blum P, Schaffitel A, Bayer P. 2013b. Long term evolution of anthropogenic heat fluxes into a subsurface urban heat island. *Environmental Science & Technology*. DOI: 10.1021/es401546u.

Molina-Giraldo N, Bayer P, Blum P. 2011a. Evaluating the influence of thermal dispersion on temperature plumes from geothermal systems using analytical solutions. *International Journal of Thermal Sciences* **50**(7): 1223–1231. DOI: 10.1016/j.ijthermalsci.2011.02.004.

Molina-Giraldo N, Bayer P, Blum P, Cirpka OA. 2011b. Propagation of seasonal temperature signals into an aquifer upon bank infiltration. *Ground Water* **49**(4): 491–502. DOI: 10.1111/j.1745-6584.2010.00745.x.

Olsson A, Grathwohl P. 2007. Transverse dispersion of non reactive tracers in porous media: a new nonlinear relationship to predict dispersion coefficients. *Journal of Contaminant Hydrology* **92**: 149–161.

Perrier F, Le Mouel JL, Poirier JP, Shnirman MG. 2005. Long-term climate change and surface versus underground temperature measurements in Paris. *International Journal of Climatology* **25**(12): 1619–1631. DOI: 10.1002/joc.1211.

Pollack HN, Huang SP, Shen PY. 1998. Climate change record in subsurface temperatures: a global perspective. *Science* **282**(5387): 279–281. DOI: 10.1126/science.282.5387.279.

Rau GC, Andersen MS, Acworth RI. 2012. Experimental investigation of the thermal dispersivity term and its significance in the heat transport equation for flow in sediments. *Water Resources Research* **48**(3): W03511. DOI: 10.1029/2011wr011038.

Smith L, Chapman DS. 1983. On the thermal effects of groundwater flow: 1. Regional scale systems. *Journal of Geophysical Research: Solid Earth (1978–2012),* **88**(B1): 593–608.

Stauffer F, Bayer P, Blum P, Molina-Giraldo N, Kinzelbach W. 2013. *Thermal Use of Shallow Groundwater*. CRC Press: Baton Rouge, FL, USA; 287 pages.

Stallman RW. 1963. Computation of ground-water velocity from temperature data. *U.S. Geological Survey. Water Supply Paper* **1544-H**: 35–46.

Suzuki S. 1960. Percolation measurements based on heat flow through soil with special reference to paddy fields. *Journal of Geophysical Research* **65**(9): 2883–2885. DOI: 10.1029/JZ065i009p02883.

Taniguchi M, Shimada J, Tanaka T, Kayane I, Sakura Y, Shimano Y, Dapaah-Siakwan S, Kawashima S. 1999. Disturbances of temperature-depth profiles due to surface climate change and subsurface water flow: 1. An effect of linear increase in surface temperature caused by global warming and urbanization in the Tokyo metropolitan area, Japan. *Water Resources Research* **35**(5): 1507–1517. DOI: 10.1029/1999WR900009.

Taniguchi M, Shimada J, Uemura T. 2003. Transient effects of surface temperature and groundwater flow on subsurface temperature in Kumamoto Plain, Japan. *Physics and Chemistry of the Earth* **28**(9-11): 477–486. DOI: 10.1016/s1474-7065(03)00067-6.

Taniguchi M, Uemura T, Jago-on K. 2007. Combined effects of urbanization and global warming on subsurface temperature in four Asian cities. *Vadose Zone Journal* **6**(3): 591–596. DOI: 10.2136/vzj2006.0094.

VDI-4640/1. 2000. Thermal use of the underground—fundamentals, approvals, environmental aspects VDI (verein deutscher ingenieure).

Voigt J, Kilian L. 2007. Grundwassermodell für das Rheinische Braunkohlerevier, in Modellbericht, RWE Power AG, Cologne.

Wang K, Lewis TJ, Belton DS, Shen PY. 1994. Differences in recent ground surface warming in eastern and western Canada: evidence from borehole temperatures. *Geophysical Research Letters* **21**(24): 2689–2692. DOI: 10.1029/94GL02670.

Yamano M, Goto S, Miyakoshi A, Hamamoto H, Lubis RF, Monyrath V, Taniguchi M. 2009. Reconstruction of the thermal environment evolution in urban areas from underground temperature distribution. *Science of The Total Environment* **407**(9): 3120–3128. DOI: 10.1016/j.scitotenv.2008.11.019.

Zhu K, Blum P, Ferguson G, Balke KD, Bayer P. 2010. The geothermal potential of urban heat islands. *Environmental Research Letter* **5**(4): 044002. DOI: 10.1088/1748-9326/5/4/044002.

SUPPORTING INFORMATION

Additional supporting information may be found in the online version of this article at the publisher's web-site.